Appl. Phys. B 64, 717–724 (1997)

Applied Physics B Lasers and Optics



# Imaging and post-processing of laser-induced fluorescence from NO in a diesel engine

**Th.M. Brugman, G.G.M. Stoffels, N. Dam, W.L. Meerts, J.J. ter Meulen**

Department of Molecular and Laser Physics, University of Nijmegen, Toernooiveld, 6525 ED Nijmegen, The Netherlands
(Fax: +31-24/365-3311)

Received: 11 July 1996/Revised version: 12 November 1996

**Abstract.** The imaging of in-cylinder NO distributions in a steadily running optically accessible diesel engine operated on standard diesel fuel is performed by means of the 2D-LIF technique and a tunable ArF excimer laser at 193 nm. Simultaneous excitation at 226 nm showed that no sizable photo-chemical effects are induced by the excimer laser. In order to account for the gradually decreasing transparency of the windows due to soot deposits and for the in-cylinder attenuation of the laser intensity, signal processing procedures for the imaged distributions are presented. In addition to the more realistic depictions of NO distributions at selected crank angles and loads resulting from these procedures, the latter are an essential step towards a quantitative interpretation of the corresponding in-cylinder NO concentrations.

**PACS:** 42.30.Va; 82.20.Wt

Diesel engines are becoming increasingly popular because of their highly efficient combustion in comparison to spark ignited engines. This high efficiency generally leads to a lower emission of $CO_2$ and as a consequence diesel-fuel-driven engines tend to contribute less to the greenhouse effect. The high temperature that results from the high pressure in the combustion chamber of a diesel engine causes the auto-ignition of the fuel/air mixture but also gives rise to the subsequent formation of NO and $NO_2$. Furthermore, the largest of the organic molecules making up the complex chemical composition of diesel fuel are easily transformed into carcinogenic coatings on the soot particles that are produced during the combustion as well. For environmental reasons the emissions of $NO_x$ and soot must be reduced drastically in order to meet the ever more stringent emission standards. However, in spite of the progress made in the modelling of the physics and the chemistry in the combustion chamber [1] the diesel combustion process is still too complex to be fully understood. In recent years the applicability of several non-intrusive laser diagnostic techniques such as LIF (laser induced fluorescence) and Mie scattering to the study of the combustion processes inside diesel engines has been widely recognized. When the fuel is doped with fluorescing tracers, 2D-LIF can be successfully applied in the study of the fuel distribution in a spark-ignition engine [2] and in the combustion chamber of a directly injected diesel engine [3]. In-cylinder soot distributions may be studied by a combination of the 2D-LII (laser induced incandescence) technique and resonant (Mie) scattering [4]. In-cylinder NO distributions have been visualized by means of 2D-LIF by Arnold et al. [5], Alataş et al. [6] and Brugman et al. [7]. Alataş et al., using a 50/50 mixture of iso-octane and tetradecane in a square combustion chamber, found evidence that the NO formation ceases at 30° to 40° ATDC (after top dead centre). In these experiments it was assumed that the LIF detection method is non-intrusive. The high excimer laser intensities used, however, may give rise to photo-chemical processes by which NO is produced or destroyed. This might result in erroneously measured NO distributions. In this work a two-colour experiment was performed on NO in a running diesel engine in order to check for the occurrence of these photo-chemical effects.

In most of the above mentioned studies the test engines were driven by low-sooting substitute fuels and operated in skip-fired mode (i.e., the combustion in the motored engine takes place only every selectable number of cycles) in order to prolong the optical transparency of the windows of the combustion chamber. However, if the measurements are to be performed in a standard diesel-fuel-driven engine under steady operating conditions, the decreasing window transparency as a result of soot deposition should be taken into account. Also, the in-cylinder attenuation of the laser sheet intensity needs to be accounted for. The objective of this study was to investigate the extent to which the applied 2D-LIF in-cylinder imaging technique in itself is capable of producing reliable and accurate results. Therefore, methods are explored by which the imaged NO-fluorescence distributions can be adjusted for the gradually decreasing transparency of the windows and the in-cylinder attenuation of the laser intensity, in order to obtain more realistic NO distributions. In addition, as a check of the reliability of the obtained NO LIF images, measurements were performed in which the laser-beam direction was reversed. When corrected for window transmission losses and laser-beam extinction, the obtained NO images should be independent of the laser beam direction.

## 1 Experimental

The laser, the engine and the intensified CCD camera are the principal elements of the experimental setup as depicted in Fig. 1. The tunable ArF excimer laser (Lambda Physik

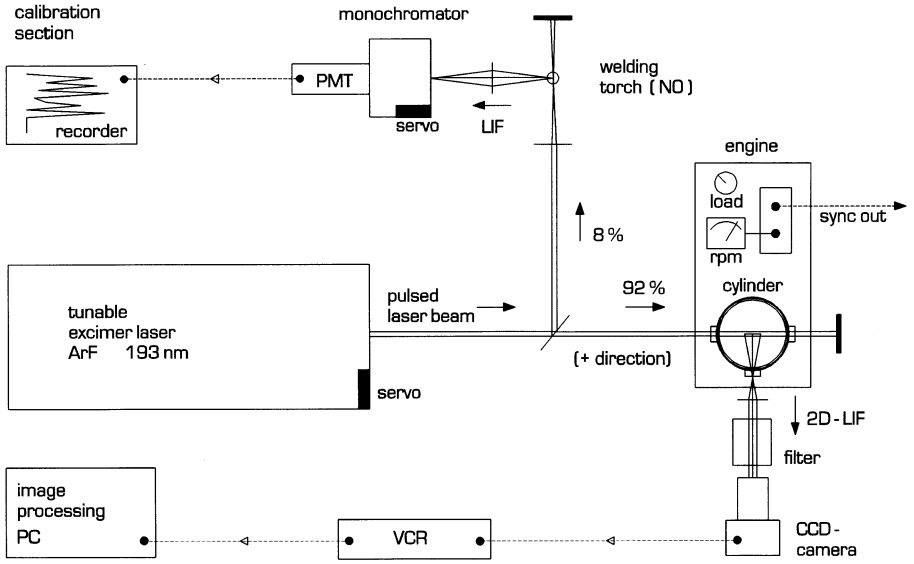


**Fig. 1.** Schematic overview of the usual experimental setup

EMG 150 MSCT) delivers 193 nm radiation with an average pulse energy of 90 mJ in 13 ns over a rectangular cross-sectional area of 75 $mm^2$ (25 mm $\times$ 3 mm). Within the 300-$cm^{-1}$-wide tuning range of the laser, NO can effectively be excited through a series of rotational lines of the vibronic band $D^2\Sigma^+(v'=0) \leftarrow X^2\Pi(v''=1)$. In a previous publication on this topic [7] excitation scans of NO in the running engine are presented. Since in the same paper the experimental setup is described in detail as well, the following is focused on the essentials and some alterations.

### *1.1 The essentials*

The 2D-LIF measurements are performed at a fixed laser wavelength (193.588 nm) corresponding to the coinciding $R_1(23.5)/Q_1(29.5)$ rotational transitions of NO in the above-mentioned band. It turns out that slightly stronger signals are obtained on these lines in comparison to the $R_1(26.5)/Q_1(32.5)$ transitions selected for imaging in [7]. Absorption of laser radiation by molecular oxygen in the Schumann–Runge band is not observed for either transition [7]. During the measurements the laser is manually kept on resonance by monitoring the simultaneously induced fluorescence from NO in an oxy-acetylene flame. In order to produce this calibration signal, about 8% of the pulse energy is focused in the flame of a welding torch by means of a beam splitter and a cylindrical lens. The LIF signal from the flame is detected by a photomultiplier attached to a monochromator set to 208 nm. This wavelength corresponds to the NO vibronic transition $D^2\Sigma^+(v'=0) \rightarrow X^2\Pi(v''=3)$. By means of two mirrors the remaining pulse energy is sent through the cylinder. This yields about 60 mJ/pulse at the location of the laser entrance window (this propagation direction is denoted by $+$). In order to verify the correction procedures the propagation direction of the laser beam through the cylinder may be reversed (this direction is denoted by $-$) by applying two more mirrors at the cost of 30 mJ/pulse, i.e., leaving 30 mJ/pulse at the opposite laser entrance window.

The cylinder of an air-cooled indirectly injected 4-stroke diesel engine (HATZ-Samofa) with a swept volume of about 580 cc (bore 86 mm, stroke 100 mm) is modified by mounting three cylindrical quartz windows (diameter 25 mm) in the cylinder wall as close to the cylinder head as possible. This construction provides optical access to the interior of the cylinder as long as the moving piston does not block the windows, i.e., for crank angles greater than 70° ATDC in the expansion stroke. Two of these three windows serve the purpose of transmitting the vertically oriented 25 mm high and 3 mm thick laser sheet, and the induced fluorescence is imaged through the third window in a direction perpendicular to the laser sheet. A spherical lens ($f = 5.5$ cm) placed directly in front of this third window increases the field of view of the imaging system. The 2D-LIF signal is separated from the resonantly scattered laser radiation by means of a 10 nm bandwidth interference filter (Laser Optik, Garbsen, Germany) adjusted to maximum transmission ($\approx 80\%$) at 208 nm. The 2D-LIF signal is then fed into the 50 ns gated image intensifier in front of the CCD camera to be recorded on video tape for later processing. The background signal proved to be negligible with this setup [7]. The spherical lens in the detection path causes all images to suffer from spherical abberations. Furthermore, growing transmission losses towards the edge of the imaged area are observed as a result of the decreasing collection efficiency of the detection system. However, the transmission in the central part of the detection path was measured to be higher than 75% within 90% of the radius of the imaged area. In this work the position of the spherical lens is fixed so as to monitor a 5 cm wide in-cylinder area.

An opto-electronic device continuously measures the crank position of the engine with an accuracy of about 1.2°. This device triggers a delay generator which in turn synchronizes the laser pulses, the LIF calibration section and the 2D-LIF imaging system. An adjustable water-cooled electric brake mounted on the flywheel of the engine provides various load conditions. Most of the NO imaging presented in this work is performed while the engine is running steadily (about 1000 rpm) on standard diesel fuel. A fixed amount of oxygen (circa 12%) is added to the inlet air of the running engine in order to raise the combustion temperature, resulting in an increased population of the probed ($v''=1$) state of NO. The increased combustion temperature also leads to decreased soot

formation, and, as a consequence, a sufficiently high optical transparency of the quartz windows can be maintained over almost unlimited periods of time. The temperature of the exhaust gases is measured using a thermocouple mounted in the exhaust pipe approximately 5 cm from the cylinder. If the engine idles (no load) this temperature is typically 250 °C; it gradually rises up to 400 °C if the load is increased to 0.8 kW. Increasing the load any further eventually leads to critical temperatures in respect of the sealings for the windows in the cylinder wall. The pressure in the cylinder for the running engine is measured by replacing one of the quartz windows by a water-cooled pressure transducer (AVL QC 32) designed for pressures up to 20 MPa at high combustion temperatures. The output of this transducer is fed into a charge amplifier, the output of which is averaged over 50 cycles by a digital oscilloscope. This set-up permits the in-cylinder pressure to be precisely monitored during the optically accessible parts of the combustion cycle.

The imaging hardware consists of an image processing board (Matrox PIP-1024 A/D converter) installed in a 486DX4 100 MHz personal computer. This board produces images with 8 bits dynamic range consisting of 512 pixels × 512 pixels. The software provides the possibility to grab these images continuously and to display each grabbed frame in a number of different false colour representations on the screen of a separate RGB monitor. In contrast to many other image processing systems this system accepts input from a standard VHS video recorder as well, thus allowing for the off-line analysis of recorded 2D-LIF signals. Another relevant software option offers the possibility to add any number of grabbed frames in order to produce an averaged image. This is achieved by dividing the 512 pixels × 512 pixels array of added intensities by the number of frames grabbed and a subsequent re-scaling of the result to the full dynamic range.

### *1.2 The measuring sequence*

Before each 2D-LIF measurement the intensity distribution of the laser sheet in the motored engine is averaged over about 300 Mie-scattered images by bypassing the interference filter in front of the CCD camera (resonant scattering by residual particles). This measurement takes about two minutes. Next, the interference filter is re-installed and a 2D-LIF measurement in the running engine is performed over the next two minutes. Immediately after the 2D-LIF measurement the engine is motored again and the averaged intensity distribution of the laser sheet is measured in the same way as before. Any locally decreased transmissions caused by the gradual build-up of local soot deposits on the windows while the engine is running is spotted by a comparison of the two averaged intensity distributions of the laser sheet before and after the 2D-LIF measurement.

### *1.3 The double resonance setup*

For the excimer laser induced fluorescence to be a reliable technique for NO detection, the excimer laser should not produce or destroy any NO by itself. In order to check that no such photo-chemical effects occur, a four-level double resonance experiment is performed, in which the NO fluorescence induced by a probe laser is monitored as a function of the presence or absence of the excimer laser. The experimental setup is schematically depicted in Fig. 2. A frequency-doubled pulsed dye laser, operated on Coumarin 47, is used as the probe laser, providing about 0.5 mJ/pulse at 226 nm (estimated pulse energy in the combustion chamber). This laser is used to excite rotational transitions in the $A^2\Sigma^+(v'=0) \leftarrow X^2\Pi(v''=0)$ band. The resulting fluorescence in the $A^2\Sigma^+(v'=0) \rightarrow X^2\Pi(v''=4)$ band at 272 nm is monitored by a gated intensified slow-scan CCD camera system (LaVision, FlameStar) through a 3 mm thick UG 5 filter. A spherical lens ($f = 30$ cm) focuses the probe laser beam at the axis of the cylinder in such a way that both laser pulses have maximum spatial overlap. When the excimer laser and the dye laser are applied together, the dye laser is delayed by 40 ns with respect to the excimer laser. This delay serves two purposes. On the one hand the excimer laser itself produces strong fluorescence at 272 nm, which, however, has decayed to a manageable level after 40 ns. Furthermore, the delay allows for equilibration of the NO population distribution following the excimer pulse, so that any

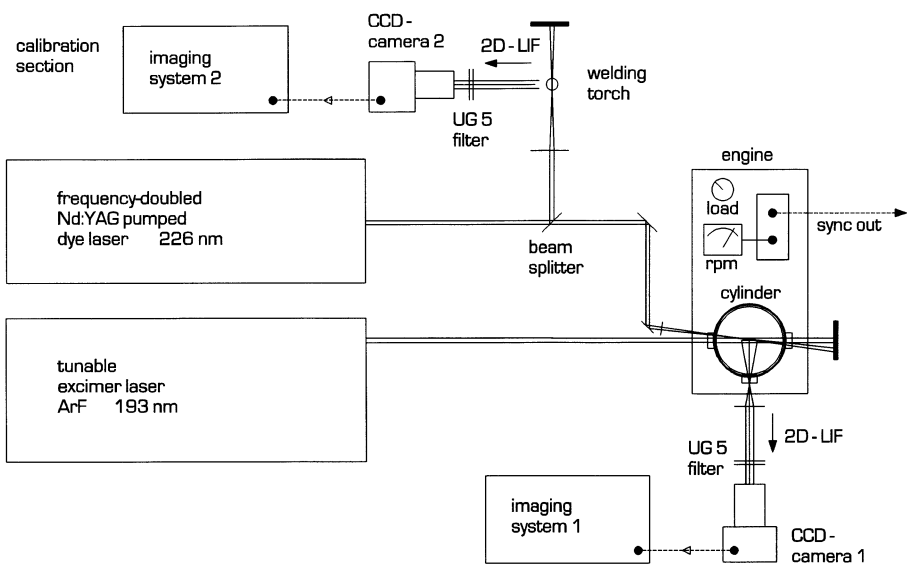


**Fig. 2.** Schematic overview of the modified experimental setup

photo-chemically induced change in the NO population might communicate itself to the level probed by the dye laser.

## 2 Signal processing

In spite of the high combustion temperature the running engine still produces enough soot to locally reduce the transmission of the quartz windows. These soot particles tend to mix with the lubricant of the engine and as a result sticky UV-absorbing deposits on the inner surfaces of the quartz windows may occur over longer periods of time. Although the initial locations of the deposits are rather unpredictable, changes in these locations during the measurements in the running engine are not observed. In fact, it turns out that after each session (taking about 45 minutes in which the engine is alternately fired and motored) the deposits can be thoroughly removed only by means of copper polish. If the laser entrance window happens to become locally blocked by these deposits the measured averaged NO-fluorescence distribution displays corresponding horizontal areas of apparently lower NO concentrations as a result of the inhomogeneous intensity distribution in the laser sheet [7]. Whenever such deposits are formed on the inner surface of the window facing the camera the imaged NO distribution might also be misleading because of the locally decreased transmission of the 2D-LIF signal. However, by measuring the intensity distributions of the laser sheet in the cylinder immediately before and after each 2D-LIF measurement the corresponding averaged NO-fluorescence distributions may easily be corrected for this effect. On top of that, the attenuation of the laser intensity in the cylinder of the running engine, means the NO-fluorescence distributions, as initially measured, always display the largest NO signal on the side where the laser sheet enters the cylinder. In the following, two correction procedures accounting for all the above-mentioned effects on the initially imaged NO fluorescence distributions will be presented.

It is not yet possible to correct for the effects of collisional quenching on the measured NO-fluorescence distributions. Owing to inelastic collisions, a considerable decrease in the number of fluorescing NO molecules is brought about and as a consequence the intensity of the induced fluorescence is reduced (quenched). This will affect the total signal strength of the observed NO LIF distributions, thus making the determination of absolute NO densities difficult. Nevertheless, a reliable qualitative picture of the NO distribution may be obtained as a function of the in-cylinder pressure and the load of the engine, as will be shown in the next section. Experiments to study the dependence of the quenching rates of the induced fluorescence on the temperature, the pressure and the gas composition are in progress.

The correction procedures discussed below are based on the assumption that the sampled 2D-LIF signal strength depends linearly on both the laser pulse energy and the NO population density in the imaged area. The pulse energy of the ArF excimer laser is high enough to possibly cause saturation effects and/or photo-chemical processes (creating or dissociating NO) which, in turn, would adversely affect the required linearity of the above mentioned dependencies. For this reason, a number of experiments have been performed to investigate the extent to which the conditions for the signal processing procedures are met in the actual experimental circumstances. The results of these tests will be given in the next section. On the basis of these results the following assumptions are justified.

– The measurements at 193 nm excitation are non-intrusive, i.e., the observed 2D-LIF signal from the probed NO molecules is not influenced by photo-chemistry.

– The 2D-LIF intensity from NO in the running engine at 193 nm excitation and steady operating conditions depends linearly on the local laser intensity.

These assumptions form the basis for the following image-processing procedures.

In general, the attenuation of both the laser intensity and the induced fluorescence inside the cylinder of the running engine may result from absorption and scattering by the multitude of different molecules and particles produced during combustion. It turns out that the attenuation due to photon absorption by NO molecules is negligible since the transmission of the laser sheet through the cylinder of the running engine is observed to be independent of the laser wavelength. Although probably not negligible, the in-cylinder attenuation of the NO LIF signal itself is expected to be more or less uniform over the imaged area. The dominant laser attenuation mechanism turns out to result from absorption and Mie scattering by particles. The resonantly scattered 2D signal will be a measure for the laser intensity distribution in the imaged in-cylinder area, provided the differently sized scattering particles are more or less uniformly distributed within the imaged area. This condition is thought to be met on the basis of the experimental results presented in the next section. It will be shown that even in the motored engine, due to the presence of many residual soot particles, the in-cylinder laser-intensity distribution can be measured this way.

The scattered intensity $S(x,y)$ from any point $(x,y)$ in the imaged area is proportional to the local laser intensity $I(x,y)$ and to the local density $n_S(x,y)$ and the cross-section $\sigma_S(x,y)$ of the scattering particles:

$$S(x,y) \sim n_S(x,y)\sigma_S(x,y)I(x,y)\,. \tag{1}$$

The laser intensity distributions $I_B(x,y)$ and $I_A(x,y)$ in the motored engine before and after the 2D-LIF measurement are reflected by the imaged Mie scattered intensities $S_B(x,y)$ and $S_A(x,y)$, respectively. Assuming that both the 2D-LIF signal and the scattered signals are attenuated in the same way, the evaluation of the fraction $S_B(x,y)/S_A(x,y)$ over the imaged area provides a numerical measure to correct the imaged NO fluorescence distribution for any locally decreased window transparency caused by soot deposits during combustion. This correction is performed by multiplying the intensity of the initially measured NO fluorescence distribution $S^0_{NO}(x,y)$ by the value of $S_B(x,y)/S_A(x,y) = I_B(x,y)/I_A(x,y)$. The result of this correction is re-scaled by a known factor, $\alpha$, to the full dynamic range of the imaging system. The resulting image then represents the NO fluorescence distribution as would be observed in the running engine if the windows were to stay perfectly clean during the measurements.

However, in order to reconstruct more realistic NO LIF distributions a correction for the attenuation of the intensity of the laser sheet in the cylinder of the running engine has to be performed as well. Theoretically, the decay of the intensity $I$ of a laser beam along its propagation direction $(x)$ in a scattering

and absorbing medium is described by:

$$I(x,y) = I(x_0,y)\exp\left(-\int_{x'=x_0}^{x'=x}[n(x',y)\sigma(x',y)]\,dx'\right), \qquad (2)$$

where $n(x,y)$ and $\sigma(x,y)$ represent the average density and the average cross-section of the absorbing and scattering particles in the medium, respectively. Evaluating the distance $x$ in terms of camera pixel units, one may write:

$$I(x+1,y) = I(x,y)\exp[-n\sigma]_{\text{eff}}(x,y), \qquad (3)$$

expressing the decay of the laser intensity per unit distance in the propagation direction. Inserting (1) and rearranging (3) yields the decay of the in-cylinder laser intensity per unit distance in terms of the Mie scattered signal $S_R(x,y)$ as measured in the running engine:

$$\exp[-n\sigma]_{\text{eff}}(x+1,y) = \frac{[n\sigma]_{\text{eff}}(x,y)}{[n\sigma]_{\text{eff}}(x+1,y)}\frac{S_R(x+1,y)}{S_R(x,y)}. \qquad (4)$$

Assuming the distribution of the scattering particles to be more or less homogeneous in the imaged area, it follows that the decay per unit distance at any location $(x,y)$ may be approximated by $S_R(x+1,y)/S_R(x,y)$. Along the path of the laser sheet, the integrated decay is evaluated by multiplying the product of all previous fractions (varying around values slightly below unity) by the fraction found at the location $(x,y)$. The actual correction for the attenuation of the laser intensity is performed by multiplying the local intensities of the input distribution (i.e., the result of the first correction procedure) by the inverted integrated decay factor found at the corresponding points in the Mie scattered images. Again, the result of this second correction is re-scaled by a known factor, $\beta$, to the full dynamic range of the imaging system.

The fully corrected result $S_{NO}(x,y)$ is calculated by the evaluation of the following expression:

$$S_{NO}(x,y) = \beta\frac{S_R(x,y)}{S_R(x_0,y)}\alpha\frac{S_B(x,y)}{S_A(x,y)}S^0_{NO}(x,y). \qquad (5)$$

Demonstrations of both correction procedures applied to two typical NO-fluorescence distributions recorded in the same session with opposite propagation directions of the laser sheet in the running engine (135° ATDC, 1000 rpm, no load) are given in Fig. 3 (+ direction) and Fig. 4 (– direction). Both figures consist of a set of eight three-dimensional representations of all images involved in the signal processing. The plots labelled A display the Mie-scattered laser-intensity distributions in the motored engine with cleaned windows $[S_B(x,y)\text{in (5)}]$. The plots labelled B are depictions of the measured NO fluorescence distributions $\left[S^0_{NO}(x,y)\text{in (5)}\right]$. The plots labelled C show the in-cylinder laser intensity distributions measured in the motored engine immediately after the NO measurements $[S_A(x,y)\text{in (5)}]$. The plots labelled D in Figs. 3 and 4 display the results of the correction procedure for locally decreased transmissions of the windows as a result of soot deposits. Comparing plot B in Fig. 4 with plot D in Fig. 4 one observes a shift in the corrected NO distribution towards the centre of the imaged area, whereas in the other direction (with apparently little window fouling) this first correction hardly affects the initially imaged NO-fluorescence distribution (plot B in Fig. 3). The plots labelled E show the Mie-scattered intensity distributions in the cylinder of the running engine. The high intensities at the laser exit sides as displayed by plots E in Figs. 3 and 4 are artefacts, most probably caused by reflections of the laser sheet at the inner surface of the laser exit window. It turns out that the overall transmission of the laser through the cylinder is about two times higher if the engine is running (≈ 20%) instead of being motored (≈ 10%). An explanation is most likely to be found in the higher in-cylinder temperature of the running engine, causing the vaporization of lubricant droplets. This may be expected to reduce the scattering losses in the cylinder of the running engine and as a result the reflections at the laser exit window are stronger than those in the motored engine. The plots labelled F are Mie-scattered images from the motored engine measured immediately after the Mie-scattering measurements in the running engine (plots E). The plots A and F are used to perform the first correction procedure on the plots E and the results are shown in plots G in Figs. 3 and 4. The latter form, in combination with the corrected NO-fluorescence distributions (plots D), the ingredients of the second correction procedure, which accounts for the decreasing laser intensity

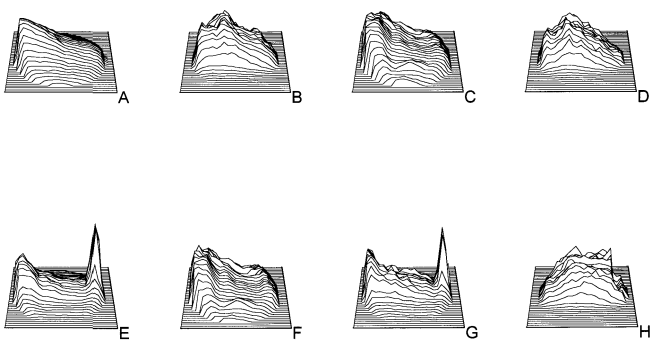


**Fig. 3.** Stages in the post-processing of NO-fluorescence images (135° ATDC). In these 3D representations the vertical axis represents the intensity over the imaged area (*xy* plane). The laser sheet travels from left to right (+ direction). See the text for the measurement sequence and the processing details. The symbols between [ ] are the ones used in (5). A: In-cylinder laser intensity distribution (derived from Mie scattering intensities) in the motored engine directly before the LIF measurement $[S_B(x,y)]$; B: NO LIF distribution $[S^0_{NO}(x,y)]$; C: As A, immediately after the LIF measurement $[S_A(x,y)]$; D: NO LIF distribution (from B) after correction for window fouling (using A and C) $[S_B S^0_{NO}/S_A]$; E: In-cylinder laser intensity distribution in the running engine $[S^0_R(x,y)]$. The spike on the right-hand side is due to a spurious reflection; F: As A, directly after the Mie measurement of E $[S_A(x,y)]$; G: In-cylinder laser intensity distribution (from E) after correction for window fouling (using A and F) $[S_B S^0_R/S_A]$; H: NO distribution (from D) after correction for laser attenuation (using G) $[S_{NO}(x,y)]$

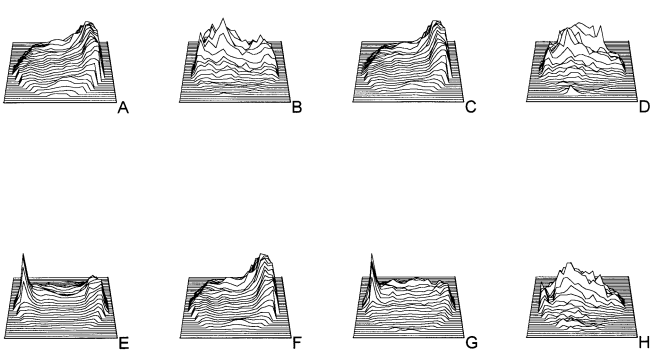


**Fig. 4.** As Fig. 3, but with the laser beam reversed (– direction)

over the field of view. Finally, the plots labelled H are depictions of the fully corrected NO-fluorescence distributions. It should be noted here that the fully processed NO distributions, like plots H in Figs. 3 and 4, typically show more centralized NO distributions in comparison to the original, uncorrected, fluorescence distributions (plots B). The effect of the 50% lower laser pulse energy in the minus direction is reflected by the noise recorded from locations below and above the laser sheet (Fig. 4, plot B). Nevertheless, after two corrections, similar in-cylinder NO-fluorescence distributions are found, independent of the propagation direction of the laser sheet. This is a strong indication for the reliability of the signal-processing procedures and the resulting in-cylinder NO distributions.

## 3 Results and discussion

### *3.1 Validation of the detection method*

*3.1.1 Two-colour excitation.* In Fig. 5 two NO excitation scans of the 226 nm region measured with the frequency-doubled dye laser in the running engine and in the welding torch, respectively, are presented. A simulated spectrum, calculated for $T = 1800$ K by using data from Reisel et al. [8] is given in the middle row. The three spectra show very good agreement. Evidently, the spectrum obtained from the engine is much weaker than the flame spectrum. The strongest rotational resonance ($P_2(22.5)$ at 226.364 nm [8]) was selected to check for any photo-chemical effects induced by the excimer laser radiation. The effect of the presence of the excimer laser radiation on the dye-laser-induced fluorescence signal strength from the running engine (BDC, 1000 rpm, no load) is depicted in Fig. 6. As can be clearly deduced from this figure, the observed influence of the excimer laser radiation does not exceed the experimental accuracy in view of the contribution of the excimer laser alone (sequence 5). On the evidence of Fig. 6, it is concluded that excimer laser induced photo-chemical processes, if they occur at all, have no observable influence on the population of the $X^2\Pi(v'' = 0)$ state under the present experimental circumstances. In view of the fast vibrational relaxation of NO [9] this most probably holds for the $X^2\Pi(v'' = 1)$ state (probed by the excitation at 193 nm) as well.

*3.1.2 Dependence of the LIF signal on laser power.* The linearity of the LIF signal strength in the running engine (BDC, 1100 rpm, 0.4 kW load) with the excimer laser pulse energy was tested in the experimental setup of Fig. 1 by using the $R_1(23.5)/Q_1(29.5)$ resonance. The result is given in Fig. 7. The data points represent averages over 50–100 laser shots and were recorded in different sessions on different days (indicated by different symbols in Fig. 7). Although there is considerable scatter, there is no evidence for non-linear behaviour of the LIF yield with laser pulse energy. In view of the irreproducible nature of the combustion itself, we believe this is a sufficient basis for the applicability of the correction methods outlined above.

*3.1.3 Saturation.* The mere linearity of the LIF signal strength with the excitation laser pulse energy does not necessarily imply that saturation is absent. An estimate of the degree to which saturation plays a role in the experiments described here, can be obtained by comparing the actual laser intensity

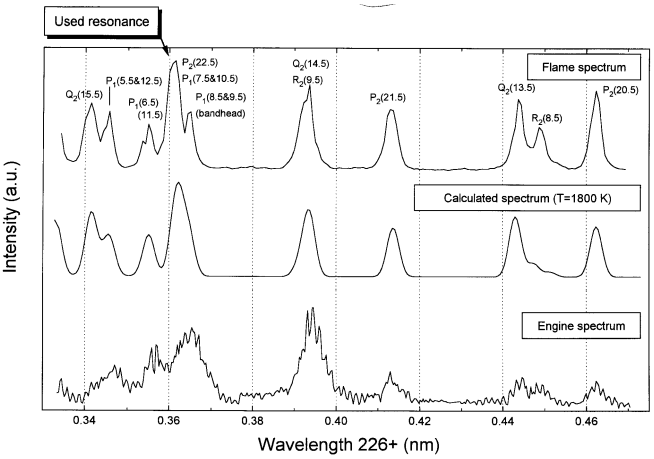


**Fig. 5.** Three NO excitation scans around 226 nm. The top scan is measured with the LaVision imaging system in the welding torch and serves as a reference scan. The $P_2(22.5)$ rotational resonance selected for the two-colour experiments in the running engine is indicated in this scan as well. The middle scan is simulated for $T = 1800$ K on the basis of data of Reisel et al. [8]. The bottom scan is measured in the running engine with the LaVision imaging system

with the saturation intensity. Assuming dominant homogeneous broadening, the saturation intensity $I_S$ is defined as [10]

$$I_S = \frac{cR_{av}\Delta\nu}{B_{12}}, \tag{6}$$

with $c$ the velocity of light, $R_{av}$ the average relaxation rate of upper and lower level, $B_{12}$ the Einstein coefficient for (stimulated) absorption and $\Delta\nu$ the laser bandwidth. Although $R_{av}$ and $B_{12}$ are not known for the D←X transition, they can be estimated. $B_{12}$ is related to the Einstein coefficient $A_{21}$ through

$$B_{12} = \frac{\lambda^3}{4h}A_{12}\,. \tag{7}$$

For the $D^2\Sigma^+(v' = 0)$ state, the electronic lifetime $\tau_{el} = 0.018\,\mu$s [11], which poses an upper limit to $A_{21}$ of

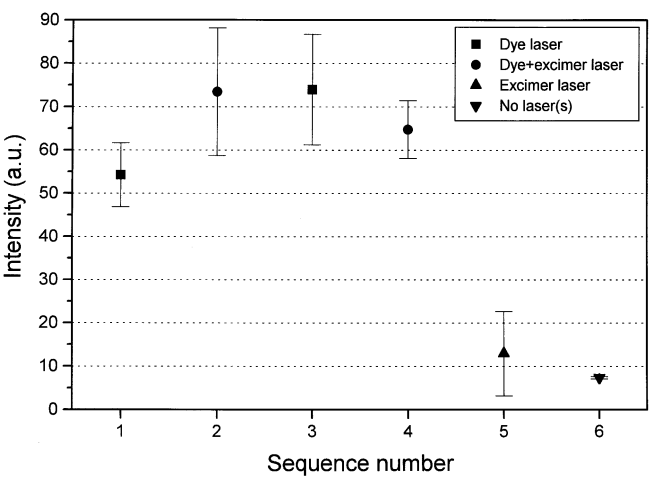


**Fig. 6.** Averaged NO 2D-LIF signal strengths at 226.364 nm dye laser excitation in the presence and the absence of 193.558 nm excimer laser excitation as measured in the running engine (BDC, 1000 rpm, no load) with the LaVision imaging system

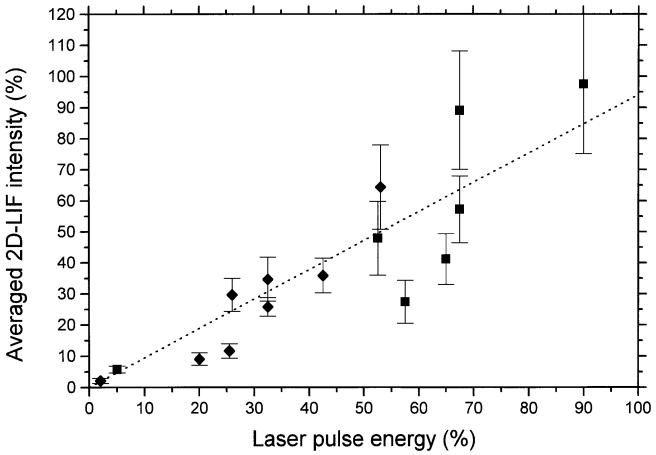


**Fig. 7.** Normalized dependence of the NO 2D-LIF intensity from the running engine (BDC, 1100 rpm, 0.4 kW load) on the excimer laser pulse energy. The dotted line represents a best linear fit through the data, with slope 0.94(8)

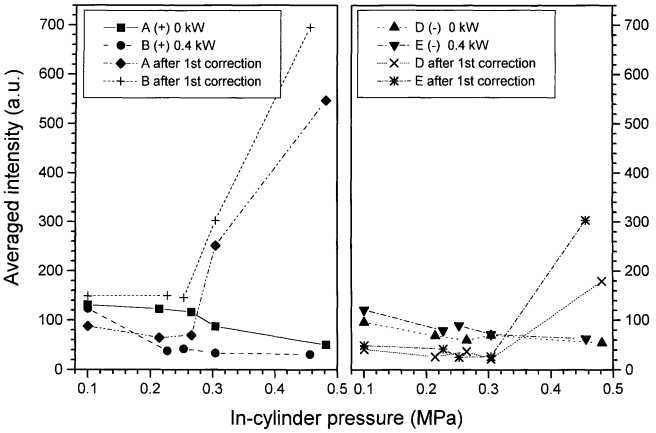


**Fig. 8.** Initially measured averaged NO fluorescence intensities per pixel for four series of measurements at the selected crank angles in both laser directions with and without a 0.4 kW load. The actual laser directions and loads are indicated in the legend. The corresponding values after the correction for soot deposits on the windows are plotted in this figure as well

$5.6 \times 10^7\,\mathrm{s}^{-1}$. If the experimentally observed linewidth of $1\,\mathrm{cm}^{-1}$ (at 1 bar) [7] is attributed solely to homogeneous broadening, this yields $R_{\mathrm{av}} \approx 6 \times 10^{10}\,\mathrm{s}^{-1}$ and this value will rapidly increase with increasing pressure. This results in $I_{\mathrm{S}} \geq 2 \times 10^9\,\mathrm{W/m}^2$ for $\Delta\nu = 0.5\,\mathrm{cm}^{-1}$, which is about five times lower than our most optimistic estimate of the in-cylinder laser intensity. Empirical direct information on the degree of saturation may be obtained from V-type three-level double resonance experiments, which are planned for the near future. It should be noted that even in the case of saturation the LIF signal strength is still linearly proportional to the local NO density.

The conditions for the correction procedures are reasonably met in the actual experimental setup. Photo-chemical reactions affecting the NO density by creation or destruction of NO molecules were not observed. The 2D-LIF signal strength depends linearly on the laser pulse energy and saturation effects affecting that linearity will probably be of minor importance.

### *3.2* NO *distributions in the running engine*

Figure 8 shows the numerical effects of the first correction procedure (for window pollution) on a number of averaged NO fluorescence intensities measured for both directions of the laser beam and at selected loads of the engine. These data are produced by bypassing the re-scalings to the full dynamic range of the imaging software [factor $\alpha$ in (5)]. Although the (second) correction for the attenuation of the laser beam remains to be performed, instead of the initially observed decay of the averaged fluorescence intensities towards higher pressures, one already observes an increase in the 2D-LIF signal strength after the first correction procedure in all four series. This is in line with the expectation that there exist higher NO densities at higher pressures. In the + direction the increase starts at 120° ATDC whereas in the − direction the corrected signal starts increasing at 105° ATDC (irrespective of the load in both cases). This difference is most probably an artefact caused by the about two times lower pulse energy of the laser in the − direction, leading to proportionally weaker 2D-LIF signals. However, as expected, in both directions the signals at 80° ATDC (around 0.47 MPa) are significantly stronger when the engine is loaded.

In Fig. 9 four initially measured NO fluorescence distributions are given in the top row and the corresponding results after both corrections are depicted in the bottom row. From left to right these distributions were measured in the + direction in the same session (lasting 30 minutes at least) at: 135° ATDC, 120° ATDC, 105° ATDC, and 80° ATDC in the expansion stroke (1000 rpm, no load), respectively. The shift in the initially measured NO-fluorescence distributions (top row) at higher in-cylinder pressures towards the side of the laser entrance window is considered to be the result of the increasing in-cylinder attenuation of the laser intensity. After both corrections the resulting NO distributions tend to shift towards the centre of the imaged area (i.e., the part of the image which suffers the least from spherical abberations) in spite of the gradual build-up of soot deposits on the observation window. The high intensities at the borders of the fully corrected distributions result mainly from inaccuracies in the second correction procedure near the image edges.

The laser intensity distributions as measured by Mie scattering in the running engine [$S_{\mathrm{R}}(x,y)$ in (5)] corresponding to the session depicted in Fig. 9, are given in Fig. 10. The evaluation of the fractions $S_{\mathrm{R}}(x,y)/S_{\mathrm{R}}(x+1,y)$ contained in these images provides a way to estimate the values of the product $[n\sigma]_{\mathrm{eff}}(x,y)$ of (3) in the running engine. This can be seen by rearranging (4) in order to obtain:

$$\frac{S_{\mathrm{R}}(x,y)}{S_{\mathrm{R}}(x+1,y)} = \frac{[n\sigma]_{\mathrm{eff}}(x,y)}{[n\sigma]_{\mathrm{eff}}(x+1,y)} \exp[n\sigma]_{\mathrm{eff}}(x+1,y)\,. \tag{8}$$

Expanding the exponential term at the right hand side and neglecting quadratic and higher order terms yields

$$\frac{S_{\mathrm{R}}(x,y)}{S_{\mathrm{R}}(x+1,y)} = \frac{[n\sigma]_{\mathrm{eff}}(x,y)}{[n\sigma]_{\mathrm{eff}}(x+1,y)} + [n\sigma]_{\mathrm{eff}}(x,y). \tag{9}$$

Since the scattering particles are assumed to be more or less homogeneously distributed, the first term on the right hand side reduces to unity. The values for $[n\sigma]_{\mathrm{eff}}(x,y)$ are then found to typically vary around $\approx 0.005$. On the evidence of this evaluation of the laser intensity distributions, the scattering particles in the running engine seem to be more or less homogeneously distributed within the imaged area indeed. Similar

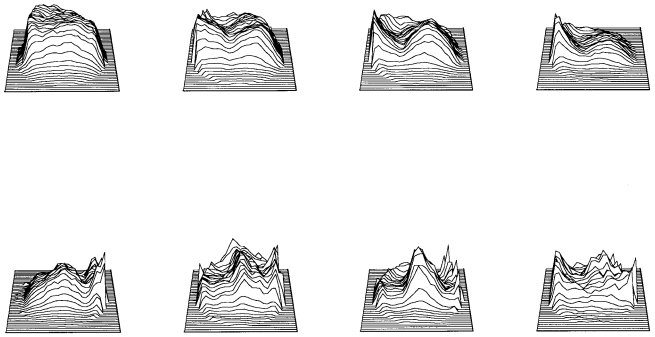

**Fig. 9.** Four representations of the initially measured NO fluorescence distributions in the + direction of the laser sheet are depicted in the top row. From left to right these distributions were measured at: 135° ATDC, 120° ATDC, 105° ATDC and 80° ATDC (1000 rpm, no load), respectively. The bottom row shows the corresponding results if the distributions of the top row are corrected for both the soot deposits and the in-cylinder laser intensity attenuation

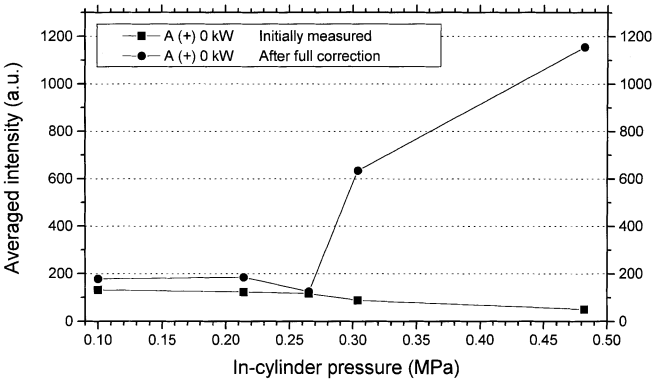


**Fig. 11.** The results of the numerical analysis performed on the averaged intensities of the initially measured NO-fluorescence distributions given in Fig. 9 before and after correction for soot deposits on the windows as well as for the in-cylinder laser attenuation

distributions and values are obtained for scattering along the – direction.

The results of the numerical analysis performed on the averaged 2D-LIF signal strength of the initially measured NO-fluorescence distributions given in Fig. 9 before and after both corrections [involving both scale factors $\alpha$ and $\beta$ in (5)] are plotted in Fig. 11. The corrected signal at 80° ATDC is about 23 times stronger than the measured 2D-LIF signal. Since the effect of collisional quenching on the signal strength is not yet known, one must be very careful in drawing conclusions about the absolute amount of NO from this figure.

## 4 Summary

Nitric oxide LIF distributions inside the cylinder of an optically accessible 4-stroke IDI diesel engine running on standard diesel fuel are presented. These NO distributions are obtained by using 2D fluorescence imaging induced by an ArF excimer laser ($\lambda \approx 193$ nm). Correction procedures were developed to take into account the effects of window fouling and in-cylinder laser attenuation due to scattering by a uniform field of soot particles. The correction procedure for window fouling is efficient enough for measurement sessions to last up to ca. 45 minutes. These numerical image processing procedures are an essential step towards the quantitative interpretation of the fluorescence distributions. In contrast to the measured NO-fluorescence distributions (the "raw data"), the processed distributions are shown to be hardly dependent on the direction in which the excitation laser traverses the engine. This is good evidence to justify the interpretation of the corrected images as relative NO density distributions.

The excimer laser itself is found not to induce observable photo-chemical effects. The LIF signal is shown to depend linearly on the laser intensity. Also, saturation is expected to play a minor role in this work.

In the range of 80° – 180° ATDC, NO is found to be located in the central part of the cylinder. Its density is found to increase with increasing load and with decreasing crank angle. The latter trend is born out of the processing of the raw data. At the current state of knowledge, a quantitative interpretation of the NO LIF signal is hampered by the lack of data on the collisional quenching of the D→X fluorescence under the conditions prevailing in a diesel engine.

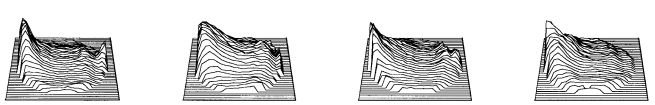

**Fig. 10.** From left to right four representations of in-cylinder laser intensity distributions in the running engine after the correction for soot deposits on the windows, are shown. The (scattered) distributions were initially imaged in the + direction at: 135° ATDC, 120° ATDC, 105° ATDC and 80° ATDC in the expansion stroke (1000 rpm, no load). These intensity distributions are actually involved in the correction for the in-cylinder laser attenuation of the NO-fluorescence distributions given in the top row of Fig. 9

*Acknowledgements.* This research is supported by the Technology Foundation (STW). The financial support of NOVEM B.V., Utrecht, The Netherlands and TNO, Delft, The Netherlands is gratefully acknowledged. The expert technical assistance of E. van Leeuwen, F. van Rijn, R. and E. Merkus is highly appreciated. Finally, P. Schmidt is acknowledged for his simulation of the 226 nm region of the NO spectrum.

## References

1. B. Dillies, K. Marx, J.E. Dec, C. Espey: SAE Paper **930074** (1993)
2. H.M. Ney, B. Johansson, M. Aldén: *Unsteady Combustion* , NATO ASI Series, (Kluwer Academic Publishers, Dordrecht, Boston, London 1993) pp. 383-389
3. J.E. Dec, C. Espey: SAE Paper **922307** (1992)
4. C. Espey, J.E. Dec: SAE Paper **930971** (1993)
5. A. Arnold, F. Dinkelacker, T. Heitzmann, P. Monkhouse, M. Schäfer, V. Sick, J. Wolfrum, W. Hentschell, K.P. Schindler: *24th Int'l Symp. on Combustion*, Sydney (1992)
6. B. Alataş, J.A. Pinson, T.A. Litzinger, D.A. Santavicca: SAE Paper **930973** (1993)
7. Th.M. Brugman, R. Klein-Douwel, G. Huigen, E. van Walwijk, J.J. ter Meulen: Appl. Phys. B **57**, 405 (1993)
8. J.R. Reisel, C.D. Carter, N.M. Laurendeau: J. Quant. Spectrosc. Radiat. Transfer **47-1**, 43 (1992)
9. M.J. Frost, M. Islam, I.W.M. Smith: Can. J. Chem. Vol. **72**, 606 (1994)
10. W. Demtröder: *Laser Spectroscopy. Basic Concepts and Instrumentation*, 2nd enlarged edn. (Springer, Berlin, Heidelberg 1995) p. 91
11. A.A. Radzig, B.M. Smirnov: Springer Series in Chem. Phys. Vol. **31**, 386 (1985)